Journal of the Ceramic Society of Japan 124 [4] 421-425 2016 Full paper

Determination of the size of representative volume element for viscous sintering

Gaku OKUMA, Daiki KADOWAKI, Yutaka SHINODA, Takashi AKATSU,* Olivier GUILLON and Fumihiro WAKAI†**

Secure Materials Center, Materials and Structures Laboratory, Tokyo Institute of Technology, R3–23 4259 Nagatsuta, Midori, Yokohama, 226–8503, Japan

***Course of Advanced Technology Fusion, Graduate School of Science and Engineering, Saga University, 1 Honjo-machi, Saga 840–8502, Japan**

****Institute of Energy and Climate Research IEK-1: Materials Synthesis and Processing, Forschungszentrum Jülich GmbH, D-52425 Jülich, Germany**

The representative volume element (RVE) is a basic concept in the continuum mechanics of sintering of random heterogeneous porous materials. A quantitative determination of its size was performed by using synchrotron X-ray microtomography data of constrained sintering of thin glass film on a rigid substrate. A RVE size is associated with a property of interest; we determined it for relative density, specific surface area, and hydrostatic component of sintering stress. The RVE size was estimated to be from 11 to 17 times larger than the average initial particle size. The RVE size was associated with a given precision of the property. It depended on the volume fraction of porous structure, or, relative density, so that it varied with microstructural evolution.

Key-words : Sintering, Micromechanical modeling, Viscous flow

[Received November 5, 2015; Accepted January 31, 2016]

1. Introduction

The macroscopic shrinkage in sintering occurs as a result of the microstructural evolution in particle scale that is driven by capillarity. The shape and form of pore structures, either open or closed, generate the thermodynamic driving force of shrinkage, i.e., sintering stress. In a macromechanical approach, the heterogeneous microstructure of the porous body is replaced by a homogeneous medium. For the macroscopically isotropic medium, the continuum mechanical modeling of sintering is expressed as[1),2)]

$$\dot{E}_{ij} = \frac{\Sigma'_{ij}}{2G} + \delta_{ij}\frac{(\Sigma_m - \Sigma^s)}{3K} \quad (1)$$

where $\dot{E}_{ij}$ is the macroscopic strain rate, Σ'_{ij} and Σ_m are deviatoric and hydrostatic components of macroscopic stress, Σ^s is the sintering stress, and G and K are the shear viscosity and the bulk viscosity, respectively. The shrinkage occurs spontaneously due to the presence of the sintering stress, even if the applied stress is zero. The sintering stress is useful also to analyze the thermal stability of porous structures,[3),4)] such as electrodes in solid oxide fuel cell at elevated temperatures.

The macroscopic properties are defined as the average over the representative volume element (RVE).[5),6)] RVE is a volume of heterogeneous material that is sufficiently large to contain enough information at the micro scale in order to be representative, but it should be much smaller than the macroscopic body, in fact as small as possible. The concept of RVE links the heterogeneities at the microscale with macroscopic quantities; this separation of scales is known as the Micro-Meso-Macro principle.[6)] Several works have investigated the existence of an RVE and the possibility to determine its size by using statistical-numerical analysis.[7)–11)] These studies intended to predict the effective mechanical properties of composites. Recent advances in X-ray microtomography[12)] and focused ion beam-scanning electron microscopy[13)] have opened the door for observation of detailed microstructural evolution during sintering, and provides an opportunity to analyze the RVE from the knowledge of microstructure experimentally. In the field of particle packing, for example, Razavi and coworkers[14)] reported that the concept of RVE provides an effective means of developing macroscopic measures in the description of granular materials. The RVE size has been determined for electrodes of a Li-ion battery[15)] and solid oxide fuel cell.[16)–18)]

Wakai and Guillon[19)] studied glass films sintered by viscous flow and imaged by X-ray microtomography in order to evaluate the sintering stress tensor from 3-D visualization of microstructure. The hydrostatic component of sintering stress in a volume element V is simply calculated from its relative density ρ and its specific surface area $S_V \equiv A_{\text{pore}}/V$ for viscous sintering[19),20)]

$$\Sigma^s = \frac{2\gamma_s S_V}{3(1-\rho)} \quad (2)$$

where γ_s is the surface energy, and A_{pore} is the surface area of pores.

In the present paper we determine the RVE size for fundamental properties in sintering: relative density, specific surface area, and hydrostatic component of sintering stress. We show that the minimum size of RVE depends on the material property and level of precision required for the analysis.

† Corresponding author: F. Wakai; E-mail: wakai.f.aa@m.titech.ac.jp

‡ Preface for this article: DOI http://dx.doi.org/10.2109/jcersj2.124.P4-1

DOI http://dx.doi.org/10.2109/jcersj2.15275

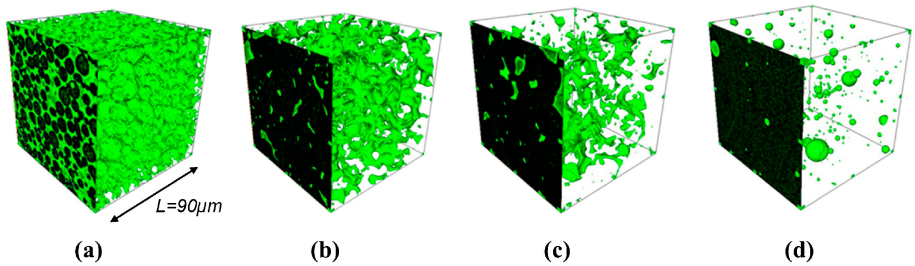

Fig. 1. Evolution of pore space in sintering: (a) stage 1 (relative density, $\rho = 63.5\%$); (b) stage 2 ($\rho = 87.8\%$); (c) stage 3 ($\rho = 94.1\%$); (d) stage 4 ($\rho = 98.4\%$).

2. Experimental

Processing of glass films from spherical particles and synchrotron X-ray microtomography has been fully described elsewhere[12] and will be only outlined here. A soda lime glass powder with average particle size of ~8 μm was used for sample preparation. Aqueous slurry was casted on alumina substrate by using a doctor blade. The thickness and relative density of the green film were 300 μm and 61.5%, respectively. Sintering was conducted at heating rate of 5°C/min up to 600°C and then 20°C/min up to 700–750°C. Isothermal times between 0 and 10 min resulted in four different densities ranging from 64 to 98%.

X-ray microtomography data have been acquired at the European Synchrotron Radiation Facility (ESRF, Grenoble, France). Radiographs were acquired by rotating the sample by steps of 0.12° until 180°. The 3-D mapping with voxel size of $0.28 \times 0.28 \times 0.28$ μm were reconstructed. The 3-D visualization and geometrical measurements were performed using Amira (VSG) in the present study. The watershed transform was used to segment the gray value image into pore and material. The pore surface was discretized using triangular meshing, from which the surface area and the pore volume were calculated.

3. Results and discussion

3.1 Microstructural evolution in viscous sintering

The pore space evolution in viscous sintering of spherical glass particles are shown in **Fig. 1**. In the initial stage [Fig. 1(a), Stage 1], the pore structure is a continuous network with numerous circular holes resulting from contacts between particles. As holes expand with the neck growth, ligaments are pinched-off, breaking the continuous network into fragments: closed pores are formed one by one in the intermediate stage [Fig. 1(b) Stage 2, and (c) Stage 3]. Complicated shaped pores become spherical in the final stage of sintering [Fig. 1(d) Stage 4].

Figure 2 shows a 2-D section extracted from the specimen in Stage 1, which is easier to examine the microstructural heterogeneity. The smallest particles have segregated at the bottom of the layer, then, we analyze the average properties of the layer in the middle region marked in Fig. 2. Sub-volumes extracted from a total material domain are restricted to cubic geometries. As many as possible independent cubes with edge length of 160, 80, 40, 20, and 10 μm were extracted from each sample for four stages. The RVE size is given by using the edge length L of cubic volume element.

3.2 Relative density, specific surface area and sintering stress

The relative density of sub-volume in each stage is plotted as a function of the edge length of cubic volume element in **Fig. 3**.

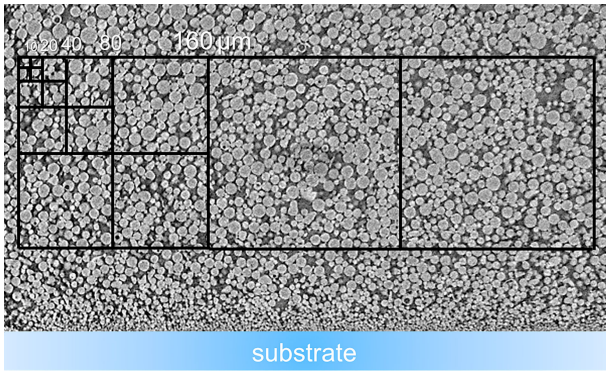

Fig. 2. Section of a sample (stage 1, relative density $\rho = 63.5\%$). The sizes of cubic volume elements are illustrated for comparison to the initial particle diameter.

Figures in brackets refer to the number of sub-volumes. The mean relative density is almost independent of edge length when sufficiently large number of sub-volumes are analyzed; the number of voxels per particle diameter was 29 in the present experiments. The scatter of data at small edge length indicates the scale of microstructural inhomogeneity. **Figures 4** and **5** show the specific surface area and the sintering stress as functions of edge length. For all three quantities the scatter of data increases with decreasing the edge length L, while their mean values were almost independent of the edge length.

Both mean value of specific surface area and that of sintering stress depends on sintering stage or mean value of relative density. The linear relation was observed between mean specific surface and mean relative density.[19] The mean sintering stress was almost constant from stage 1 to stage 3, and decreased slightly at the final stage. In the final stage of sintering, where closed pores are dispersed sparsely, the macroscopic sintering stress is dominated by the largest residual pores.[20] The mean sintering stress decreased in stage 4, because the coarsening in pore structure resulted in residual pores more than two times larger than the initial particle size as shown in Fig. 1(d).

Standard deviation for given edge length is shown in **Fig. 6**, as a function of L. It can be seen that the standard deviation is quite large for a small L; it decreases as L increases, and converges to a constant value. The variation of standard deviation on L reflects the microstructural heterogeneity. We may assign the edge length L_r, above which the heterogeneity no longer affects the standard deviation, as the minimum size of the RVE. From this definition the RVE size is estimated to be from 90 to 135 μm for relative density, specific volume, and sintering stress. Here, the non-dimensional RVE size L^* is defined as

$$L^* = L/d \tag{3}$$

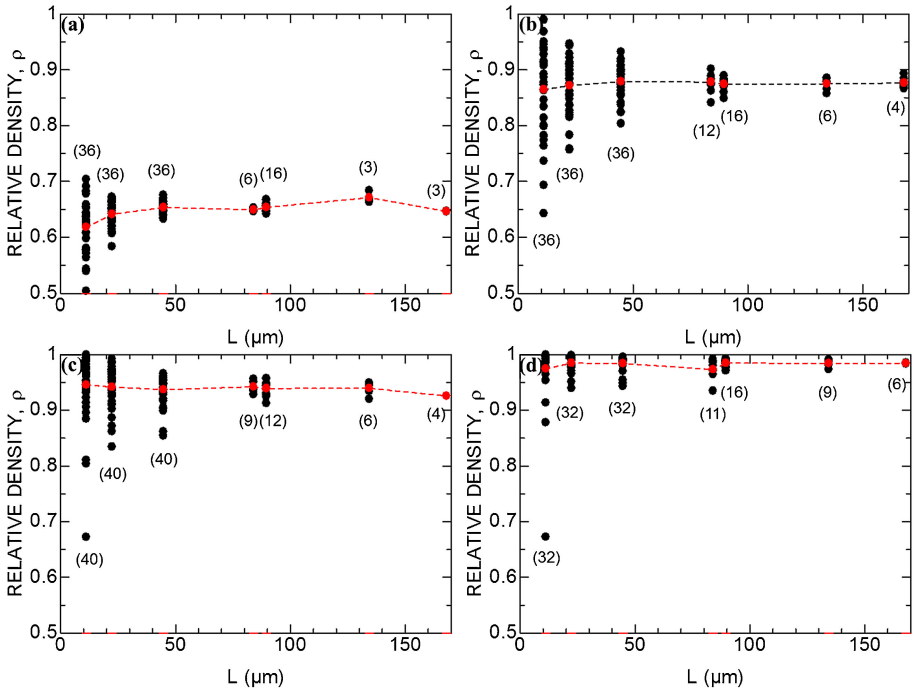

Fig. 3. Relative density of each volume element: (a) stage 1, (b) stage 2, (c) stage 3, (d) stage 4. The dotted line shows the mean value.

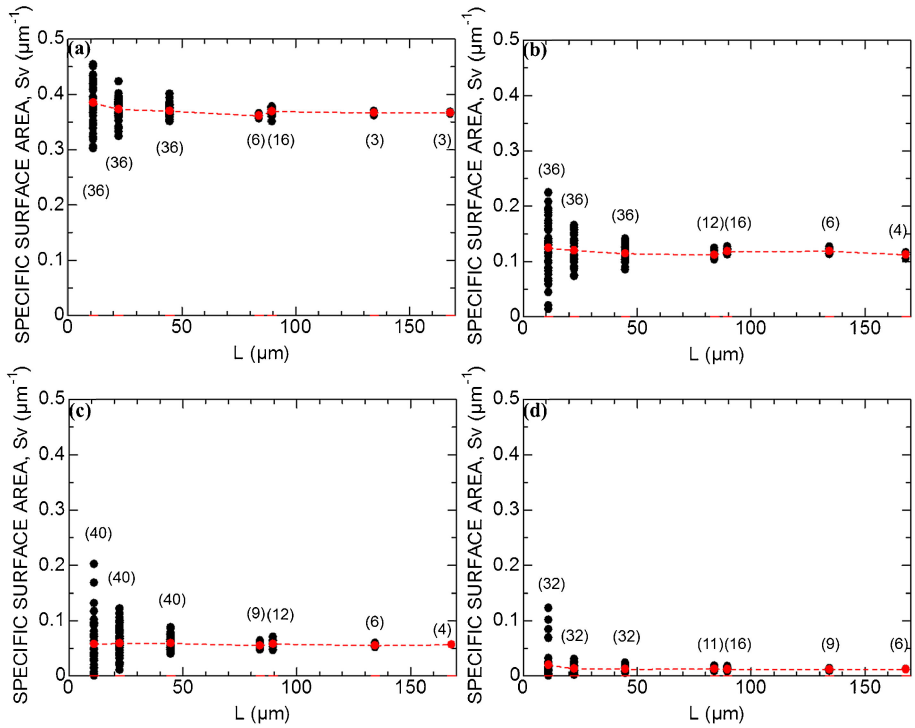

Fig. 4. Specific surface area of each volume element: (a) stage 1, (b) stage 2, (c) stage 3, (d) stage 4. The dotted line shows the mean value.

where d is the average initial particle size (8 μm). The non-dimensional RVE size was from 11 to 17 in the present experiments. This result agrees with the values reported for granular materials.[14] However, this normalization is done with respect to the initial microstructure, which completely disappears during sintering.

Alternatively the RVE size can be defined from standard deviation-edge length curves. Since both mean value and standard deviation of each quantity varies with relative density, we normalized standard deviation by the mean value at stage 1 ($\rho = 63.5\%$). The RVE size was defined with the normalized standard deviation; either 5 or 2% for the RVE size of relative

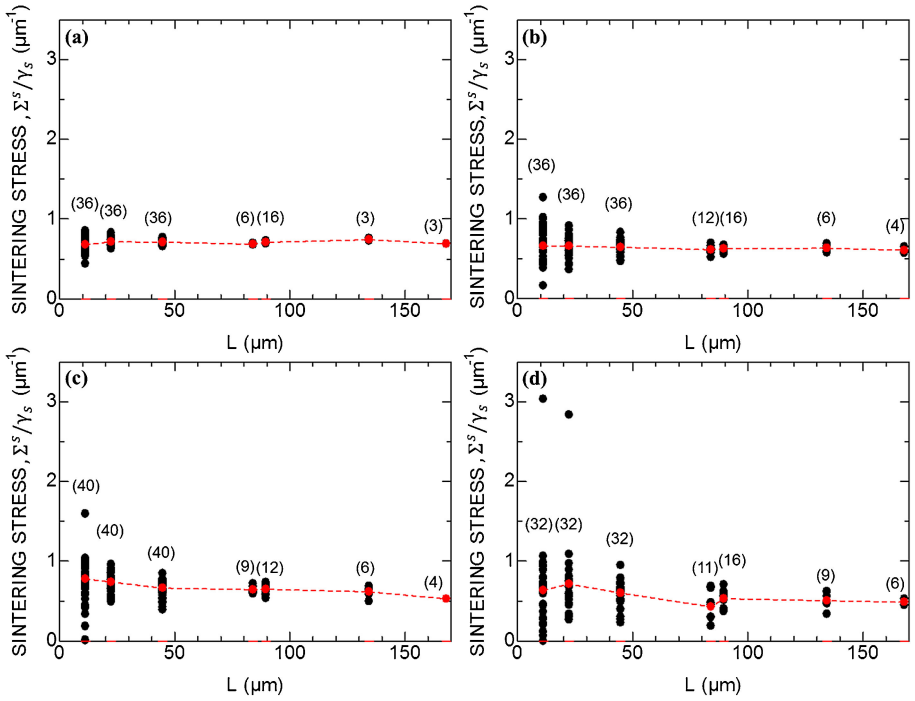

Fig. 5. Sintering stress of each volume element: (a) stage 1, (b) stage 2, (c) stage 3, (d) stage 4. The dotted line shows the mean value.

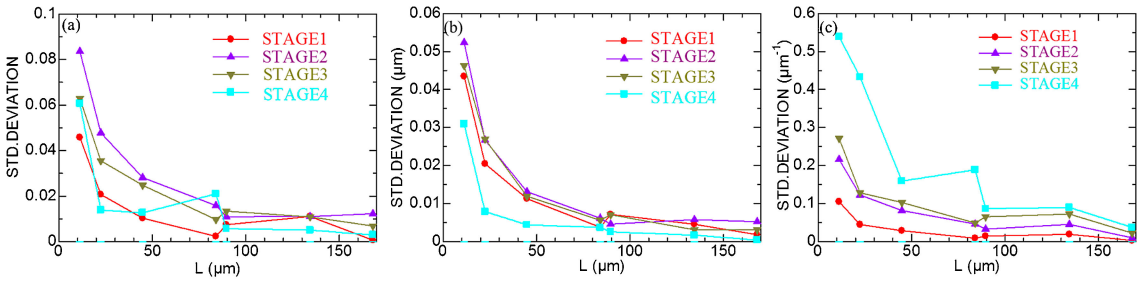

Fig. 6. Standard deviation as a function of the edge length of cubic elements: (a) relative density, (b) specific surface area, (c) sintering stress.

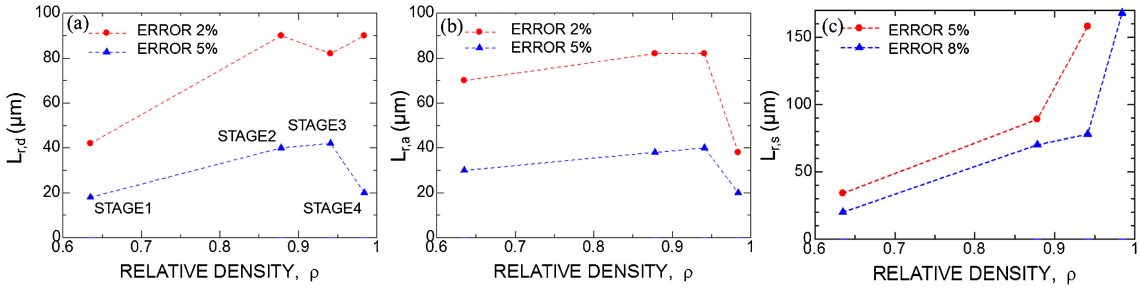

Fig. 7. RVE size as a function of relative density. (a) relative density ($L_{r,d}$), (b) specific surface area ($L_{r,a}$), and (c) sintering stress ($L_{r,s}$).

density $L_{r,d}$ and specific surface area $L_{r,a}$, and either 8 or 5% for that of sintering stress $L_{r,s}$. The RVE size was plotted as a function of relative density in **Fig. 7**. The RVE size must be larger when the desired accuracy is higher. The RVE size of relative density [Fig. 7(a)] is relatively small in stage 1 where inhomogeneities can be envisioned as local fluctuation caused by differences in random particle packing. However, larger RVE size in the later stages suggests that the characteristic length to describe microstructural heterogeneity increases from the particle size to the distance between coarse spherical pores during the microstructural evolution. The increase in the characteristic length can be called coarsening in a broad sense. The RVE size of specific surface area [Fig. 7(b)] decreased at stage 4. We suppose it is an artifact due to the definition of $L_{r,a}$ from the normalized

standard deviation, because the mean value of specific surface area and also its standard deviation approach to zero at the final stage of sintering. The RVE size of sintering stress [Fig. 7(c)] increased with densification. The scatter of sintering stress in each volume element increases with the relative density ρ, because the sintering stress is inversely proportional to porosity $1 - \rho$ which is close to zero in the final stage. Since the sintering stress is dominated by the largest pores, the RVE size for sintering stress is related to the average distance between large pores in the final stage.

4. Conclusions

The microstructural evolution of thin glass film during constrained sintering on a rigid substrate, imaged by synchrotron X-ray microtomography, was analyzed to evaluate fundamental quantities, i.e., relative density, specific surface area, and sintering stress. These parameters are important for the continuum mechanical description of viscous sintering. The minimum size of RVE was defined as the edge length of cubic volume elements above which the heterogeneity no longer affects the standard deviation. The RVE size was estimated to be from 11 to 17 times larger than the average initial particle size. Alternatively the RVE size was defined from the value of normalized standard deviation. The RVE size increased when the desired accuracy was higher. The RVE size was dependent on relative density, and varied with microstructural evolution. The relationship between RVE size and relative density was dependent on the physical property of interest.

Acknowledgements This work was supported by Japan Society for the Promotion of Science (Grants-in-Aid for Scientific Research (A) #26249110).

References

1) R. K. Bordia and G. W. Scherer, *Acta Metall.*, **36**, 2393–2397 (1988).
2) R. M. McMeeking and L. T. Kuhn, *Acta Metall. Mater.*, **40**, 961–969 (1992).
3) F. Wakai, Y. Shinoda and T. Akatsu, *Acta Mater.*, **52**, 5621–5631 (2004).
4) F. Wakai and Y. Shinoda, *Acta Mater.*, **57**, 3955–3964 (2009).
5) R. Hill, *J. Mech. Phys. Solids*, **11**, 357–372 (1963).
6) Z. Hashin, *J. Appl. Mech.*, **50**, 481–505 (1983).
7) W. J. Drugan and J. R. Willis, *J. Mech. Phys. Solids*, **44**, 497–524 (1996).
8) K. Kanit, S. Forest, I. Galliet, V. Mounoury and D. Jeulin, *Int. J. Solids Struct.*, **40**, 3647–3679 (2003).
9) I. M. Gitman, H. Askes and L. J. Sluys, *Eng. Fract. Mech.*, **74**, 2518–2534 (2007).
10) C. Pelissou, J. Baccou, Y. Monerie and F. Perales, *Int. J. Solids Struct.*, **46**, 2842–2855 (2009).
11) W. M. Harris and W. K. S. Chiu, *J. Power Sources*, **282**, 552–561 (2015).
12) D. Bernard, O. Guillon, N. Combaret and E. Plougonven, *Acta Mater.*, **59**, 6228–6238 (2011).
13) S. Hara, A. Ohi and N. Shikazono, *J. Power Sources*, **276**, 105–112 (2015).
14) M. R. Razavi, B. Muhunthan and O. A. Hattamleh, *Geotech. Test. J.*, **30**, GTJ100164 (2007).
15) P. R. Shearing, L. E. Howard, P. S. Jørgensen, N. P. Brandon and S. J. Harris, *Electrochem. Commun.*, **12**, 374–377 (2010).
16) J. Joos, M. Ender, T. Carraro, A. Weber and E. Ivers-Tiffée, *Electrochim. Acta*, **82**, 268–276 (2012).
17) J. Laurencin, R. Quey, G. Delette, H. Suhonen, P. Cloetens and P. Bleuet, *J. Power Sources*, **198**, 182–189 (2012).
18) W. M. Harris and W. K. S. Chiu, *J. Power Sources*, **283**, 622–629 (2015).
19) F. Wakai and O. Guillon, *Acta Mater.*, **66**, 54–62 (2014).
20) F. Wakai, *Acta Mater.*, **61**, 239–247 (2013).